



Accepted Article

Title: Effect of Bulky Side Group on Donor and Acceptor Interactions and its Photoemission

Authors: Kai Lin Woon, S. A. S. Mustapa, Nor Shafiq Mohd Jamel, V. S. Lee, M. Z. Zakaria, and A. Ariffin

This manuscript has been accepted after peer review and appears as an Accepted Article online prior to editing, proofing, and formal publication of the final Version of Record (VoR). This work is currently citable by using the Digital Object Identifier (DOI) given below. The VoR will be published online in Early View as soon as possible and may be different to this Accepted Article as a result of editing. Readers should obtain the VoR from the journal website shown below when it is published to ensure accuracy of information. The authors are responsible for the content of this Accepted Article.

To be cited as: *ChemPhysChem* 10.1002/cphc.202000612

Link to VoR: <https://doi.org/10.1002/cphc.202000612>

ARTICLE

Effect of Bulky Side Group on Donor and Acceptor Interactions and its Photoemission

K.L. Woon,^{[a]*} S. A. S. Mustapa^[a], N. S. MohdJamel^[b], V. S. Lee^[b], M. Z. Zakaria^[b] A. Ariffin^[b]

[a] Low Dimensional Material Research Centre,
Department of Physics,
University Malaya,
Kuala Lumpur,
Malaysia
* Corresponding authors E-mail: ph7klw76@um.edu.my

[b] Department of Chemistry,
Faculty of Science,
University Malaya,
Kuala Lumpur,
Malaysia

Supporting information for this article is given via a link at the end of the document.

Abstract: Material designs that use donors and acceptors are often found in organic optoelectronic devices. Molecular level insight into the interactions between donors and acceptors are crucial for understanding how such interactions can modify the optical properties of the organic optoelectronic materials. In this paper, tris(4-(tert-butyl)phenyl)amine (*p*TPA) was synthesized as a donor in order to compare with unmodified triphenylamine (TPA) in donor-acceptor system by having 2,4,6-triphenyl-1,3,5-triazine (TRZ) as an acceptor. Dimerization of donors and acceptors occurred in solvent when the concentration of solute is high. At 0 K, using polarizable continuum model, the nitrogen atom of TPA is found to stack on top of the center of triazine of TRZ while such alignment is offset in *p*TPA and TRZ. We attributed such alignment in TPA-TRZ as the result of attractive interaction between partial localization of 2p_z electrons at the nitrogen atom of TPA and π deficient of triazine in TPA-TRZ. By taking account random motions of solvent effect at 300 K in quantum molecular dynamics and classical molecular dynamics simulations to interpret the marked difference in emission spectra between TPA-TRZ and *p*TPA-TRZ, it was revealed that the attractive interaction between *p*TPA and TRZ in toluene is weaker than TPA and TRZ. Because of the weaker attractive interaction between *p*TPA and TRZ in toluene, the dimers adopted numerous ground state conformations resulting in broad emission superimposed with multiple small Gaussian peaks. This is in contrast to TPA-TRZ which has only one dominant dimer conformation. This study demonstrates that the strength of intermolecular interactions between donors and acceptors should be taken into consideration in designing supramolecular structure.

Introduction

Supramolecules are molecular complexes where their physical properties go beyond the mere sum of the constituent molecules depending on how the constituent molecules interact. These interactions can be categorized into π - π , CH- π , cation- π , OH or ON- π and lastly lone-pair- π interactions [1]. Such interactions can modify the structure-property relationship in supramolecules. For example, π - π stacking interactions can result in formation of triplet excimers [2,3] and lower the singlet and triplet energies of

the molecules [4,5]. When such interactions are strong, self-assembled supramolecules can be formed [6,7] as seen in deoxyribonucleic acid [8] and liquid crystals [9]. Lone-pair- π interactions have been speculated to occur in supramolecular structure in the biological systems [10-11]. Some heteroaromatic molecules are intrinsically π deficient such as 1,3,5-triazine which is speculated to give rise to lone-pair- π interactions with water molecules and amine [12] and formation of new supramolecular networks and crystal structures [13,14]. Intrinsically π deficient conjugated systems along with electron rich molecules are often used in organic photovoltaics [15,16] and organic light emitting diodes that made use of thermally activated delayed fluorescence molecules (TADF) [17,18]. Both are important classes of photoactive materials. However, whether such interactions can modify the optical properties of the supramolecules are not well studied. It is reported that lone-pair- π interactions in 1-D naphthalene diimide can modify the photochromic behaviors [19]. Recently, through space charge transfer in TADF molecules have gained interests [20-22]. A study of how interactions between spatially separated donor and acceptor influence the optical properties of the system can shield light on the characters of heteroaromatic molecules and supramolecules required for their design. Hence, we use triphenylamine (TPA) as a donor and 2,4,6-triphenyl-1,3,5-triazine (TRZ) as an acceptor to be the model molecules. We functionalized the TPA with *tert*-butyl group as a bulky side group (*p*TPA) to weaken the interactions with the assumption that it will increase the intermolecular distance. We mixed TRZ and TPA or *p*TPA at molar ratio in a solvent and we observed that emissions from the TPA-TRZ and *p*TPA-TRZ are drastically different. Through quantum molecular dynamic simulations, we found that *p*TPA-TRZ adopted several broad molecular conformations compared with TPA-TRZ resulting in different photoluminescence spectra.

Results and Discussion

Figure 1 shows the structure of the molecules used in this study. 1,3,5-triazine ring can both act as π -acceptor and σ -donor. The σ -donor originated from the sp² lone pair electrons located at the

ARTICLE

nitrogen atom in the plane of the ring. The π -acceptor originated from strong electronegativity difference between carbon and nitrogen atoms. However, in TRZ, the phenyl moieties attached to the triazine effectively shield it from interactions with other molecules leaving only the π -deficient acceptor.

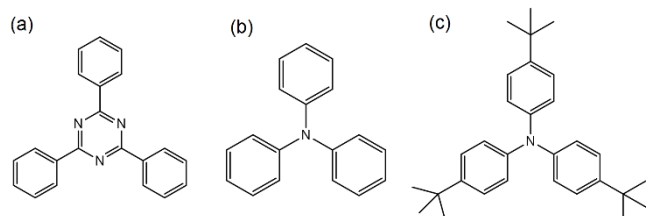


Figure 1(a): Molecular structures of (a) 2,4,6-triphenyl-1,3,5-triazine (TRZ) (b) triphenylamine (TPA) (c) tris-(4-tert-butylphenyl)amine (*p*TPA)

The more negative the electrostatic surface potential (ESP) over the centre of the aromatic ring, the stronger will be the interaction. In TPA, the central nitrogen atom formed three co-planar N-C bonds via sp^2 -hybridization leaving a valence lone pair electrons on the $2p_z$ orbital. The 3 benzene rings of TPA are not coplanar. It is twisted by $\sim 42^\circ$ from the plane leaving lone pair $2p_z$ electrons at the nitrogen atom. Because of the lack of co-planarity, the $2p_z$ lone pair of electrons cannot be fully delocalized into the π orbitals of the benzene rings resulting in 1.72 occupancy as analysed using natural bond orbitals at B3LYP/cc-pVDZ level for both TPA and *p*TPA. Functionalizing TPA with tris-(4-tert-butyl) has no influence on the lone pair occupancy. The ESP on the molecular surface is an effective means to analyse and predict noncovalent interactions. In TRZ, there is a region of negative surface potential above and below the ring, arising from the π deficient electrons.

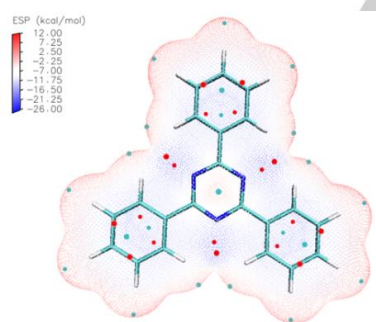


Figure 2: The colour-filled ESP on van der Waals surface based on the output of Multiwfn.

Figure 2 shows the colour-filled ESP on van der Waals surface based on the output of Multiwfn [23,24]. The grid spacing was set to 0.2 Bohr with isosurface of $q = 0.001 \text{ e/bohr}^3$. The red and the green dots represent the local surface minima and maxima respectively. The sp^2 lone pair of triazine create a negative electrostatic potential with ESP energy of -17.2 kcal/mol (blue mesh-contour). One of the local maxima is located at π deficient triazine with an ESP value of $+8.6 \text{ kcal/mol}$. Also note that local maxima can be found in the center of phenyl rings, but the ESP energy is about -10.1 kcal/mol which is far from being electron

deficient. The full list of ESP energy for corresponding surface maxima and minima can be found in supplementary information Figure S1.

Figure 3(a) shows the optimized structure of TPA-TRZ in toluene along with their combined ESP. It is clear that the center of 1,3,5-triazine ring in TRZ is stacked on top of the nitrogen atom of the TPA. One of the local maxima as indicated as a big red dot of TRZ is adjacent with the one of the local minima in TPA (big green dot). The ESP energy of the electron deficient triazine is now $+1.59 \text{ kcal/mol}$ and the nitrogen atom in TPA has an ESP energy of -12.2 kcal/mol . The presence of the minimum potential at nitrogen atom in TPA indicates a degree of localization of $2p_z$ electrons. Because of the local minima and maxima locations, we suspected that in Fig 3(a), the structure is stabilized by interaction between the partial localization of $2p_z$ electrons in TPA and the π deficient ring in TRZ. Interaction energy is obtained by calculating the total energy of the dimer subtracted by energy of each molecules. Interaction energy of -1.95 kcal/mol is obtained between TPA and TRZ. The interaction energies between various organic compounds with water stabilized by lone pair- π deficient ring have been found to be around $\sim 2 \text{ kcal/mol}$ [12]. We also need to consider the possibility of Fig 3(a) is a ground state electron-donor-acceptor complex where a fraction of charge has transferred from the TPA to TRZ. In order to calculate the fraction of electronic charge transfer at the ground state, we used atomic dipole moment corrected Hirshfeld (ADCH) population method [25]. The complex (TPA-TRZ) is divided into TPA and TRZ. The ADCH charge in TPA and TRZ alone is compared with the complex. From the analysis, we can see that TPA has acquired $0.053 |e|$ while TRZ has lost in equal amount in the complex. This is far lower than the typical value ($\sim 0.2|e|$) usually found in donor-acceptor complexes [26]. The charge transfer interaction will be minimal.

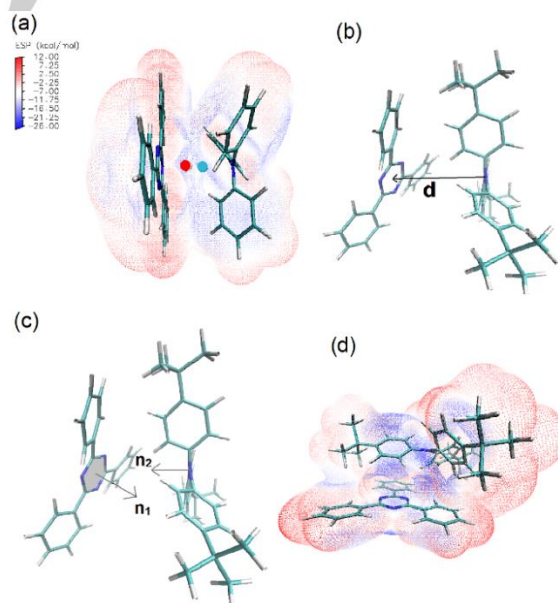


Figure 3. (a) The optimized structure of TPA-TRZ in toluene obtained at 0K along with their combined ESP. (b) The intermolecular distance is defined as distance between the centre of the triazine ring to the nitrogen atom in the TPA. (c) The normal of the plane created by the two-line vectors between adjacent nitrogen atoms in the triazine ring (shaded area) and the direction of $2p_z$ orbital of the nitrogen atom in TPA. (d) The optimized structure of *p*TPA-TRZ in toluene along with their combined ESP.

ARTICLE

The intermolecular distance is defined as the distance between the center of the triazine ring in TRZ to the nitrogen atom of TPA/*p*TPA as shown in Figure 3(b). The intermolecular distance between TPA and TRZ is 4.99 Å. The value we obtained is at the lower end of the limit. The angle is defined as an enclosed angle between normal vectors formed by the planes created by the two-line vectors between adjacent nitrogen atoms in the triazine ring and the direction of 2p_z orbital of the nitrogen atom in TPA/*p*TPA as shown in Figure 3(c). The angle for TPA-TRZ is 0.35°. However, for *p*TPA-TRZ, the center of triazine ring of TRZ is located at one of the phenyl of TPA with distance of 3.82 Å and interaction energy of -3.01 kcal/mol. The angle for *p*TPA-TRZ is 4.1°. Supposedly, by functioning TPA with bulky side group, the intermolecular distance between *p*TPA and TRZ should be further away, however, this is not the case here. The Highest Occupied Molecular Orbital (HOMO) of TPA is -5.13 eV while the *p*TPA is -4.90 eV indicating that the bulky side group acts as an electron donating group and the change is too small to result in stronger donor and acceptor interaction compared with TRZ with HOMO of -6.80 eV which is very deep. ADCH analysis also indicated negligible charge transfer at the ground state for *p*TPA-TRZ. However, the off-set alignment of *p*TPA with respect of triazine ring indicates that other forces of attraction might contribute the decrease in interaction energy. It is important to note that interaction energy consists of various contributions including van der Waals, π-π stacking, Pauli repulsion, electrostatics in origin and just to name a few. The electrostatics can be originated from electron rich and electron deficient part of the molecules such as in hydrogen bonding and even lone-pair – π interactions. Although the bulky side group of TPA exerts 'steric repulsion' or 'van der Waals repulsion' and can affect how the *p*TPA stacks on top of TRZ, the decrease of interaction energy must be attractive in nature. Hence, one possible force is van der Waals forces of attraction since there is an increase in surface area of interaction between *p*TPA and TRZ as the bulky side groups from TPA appears to interact with the phenyl group in TRZ as seen in Figure 3(d).

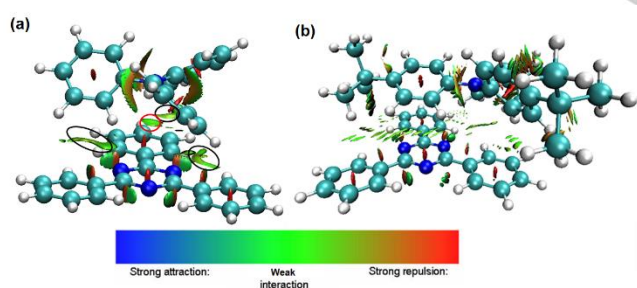


Figure 4. (a) The four regions of attractive intermolecular interactions for TPA-TRZ. (b) The interactions are more complicated consisting of interaction between 1,3,5-triazine-phenyl and tris-4-tert-butyl-phenyl interaction.

Reduced density gradient can be used to visualize the weak interaction region [27]. For TPA-TRZ, there are four regions of attractive intermolecular interactions as shown in Figure 4(a). Three of the regions correspond to off-alignment phenyl-phenyl interactions (a type of π-π interaction) as indicated in black circle while the red circle is the partial localization of 2p_z electrons -π deficient interaction. In Figure 4(b), we can see that the interactions are more complicated consisting of interaction

between 1,3,5-triazine-phenyl and tris-4-tert-butyl-phenyl interactions. One thing is certain, the partial localization of 2p_z electrons-π deficient interaction has disappeared. This is due energetic unfavorable positioning/packing of the bulky side group when the nitrogen atom in *p*TPA is stacked on top of π deficient triazine.

Figure 5(a) shows the photoluminescence spectra of the solutions of *p*TPA-TRZ in toluene at different concentrations. We can see that as concentration of *p*TPA-TRZ increases, the lower emission spectra are broadened superposed with multiple Gaussian peaks. In Figure 5(b), we compare the spectra between *p*TPA-TRZ and TPA-TRZ at 15 mM. The first peak below 400 nm is contributed by emission from TPA or *p*TPA while the lower peak at 500 nm for TPA-TRZ is originated from the dimerization of TPA and TRZ [28]. TRZ is a non-emissive molecule even excited at 300 nm.

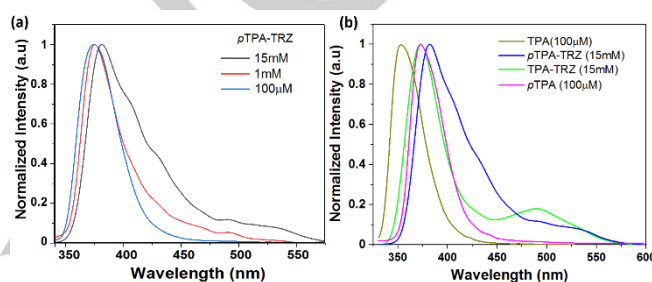


Figure 5. (a) The photoluminescence spectra of *p*TPA-TRZ at different concentrations in toluene as a solvent. (b) The spectra difference between *p*TPA-TRZ and TPA-TRZ at 15 mM.

Functionalizing the TPA with tris-4-tert-butyl red-shifted the emission peak from 354 nm to 374 nm as expected as tris-4-tert-butyl is slightly electron donating. Using cyclohexane as a solvent, multiple Gaussian peaks can also be seen in emission spectra. A new weak absorption peak can be seen at 390 nm and 425 nm in cyclohexane and toluene respectively (see supplementary information Figure S2). At first glance, the multiple Gaussian peaks as seen in *p*TPA-TRZ seem to display similar patterns with vibronic progression. Since we know that the emission is contributed by the dimerization of *p*TPA and TRZ, there is little reason to suggest the lack of vibronic progression in TPA-TRZ. However, we know that organic molecules can adopt various conformations in solvents in particular the weakly bounded dimer where solvent collisions can have sufficient energy to weaken or destroy the bounded state. Figure 3 represents the optimized structure of the molecules at 0K under implicit solvent model. It is well-known that solvent temperature can affect the structural properties of bio-molecules by controlling their flexibility [29]. Sufficient knowledge regarding the intermolecular forces are needed to predict and accurately estimate their configurations of dimer in solvent. In this paper, the relative populations of various conformers with the accuracy of quantum molecular dynamics (QMD) and inclusion of solvent under polarizable continuum model using density functional theory (DFT) are performed.

The relative populations are then estimated from the resulting residence times such that probability density mapping of the TPA-TRZ and *p*TPA-TRZ in terms of radial and the angular distribution can be plotted as shown in Figure 6. In comparison of distribution of energy obtained in Figure 6(a) and Figure 6(b), the energy for the structure in Figure 3(a) and Figure 3(b) are at the very low end

ARTICLE

of the distributions which are ~ 2.3 eV and 1.5 eV lower than the mean energy of the respective populations (see supplementary information Figure S3). As we can be seen in Figure 6(a), the ground state of TPA-TRZs tend to concentrate at about 7 Å at an angle of $\sim 55^\circ$ in contrast to *p*TPA-TRZ (Figure 6(b)) which, surprisingly, has a shorter intermolecular distance ~ 5.5 Å and an angle of $\sim 10^\circ$ (see supplementary information Figure S4 for a list of molecular configurations).

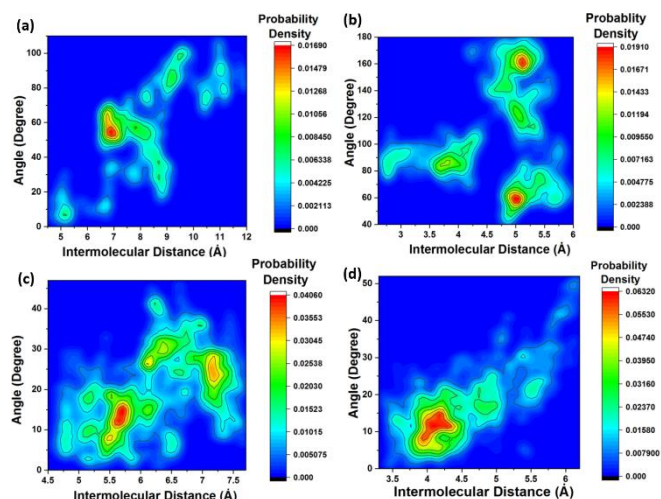


Figure 6. (a) The ground state TPA-TRZ probability density distribution versus radial angle at 300K for molecule having initial configuration of (7 Å, 55°). (b) The ground state of *p*TPA-TRZ probability density distribution versus radial angle for molecular initial configurations of (5.5 Å, 15°). (c) The excited state of TPA-TRZ probability density distribution versus radial angle for molecular initial configurations (7 Å, 55°). (d) The excited state of *p*TPA-TRZ probability density distribution versus radial for molecular initial configurations (5.5 Å, 15°)

The complexes also tend to spread into a wider distribution with two lower preferences at ~ 6.5 Å and ~ 7.5 Å with both at an angle of $\sim 25^\circ$. A molecular configuration obtained from the QMD representing each preferential orientation in ground state is sampled for interaction energy calculations. The interaction energy for TPA-TRZ is ~ -1.21 kcal/mol which is ~ 0.74 kcal/mol lower than the 0K TPA-TRZ optimized ground state. For *p*TPA-TRZ, the interaction energies at the three different preferential orientations are -0.13 kcal/mol (~ 5.5 Å, $\sim 15^\circ$), -0.06 kcal/mol (~ 6.5 Å, $\sim 25^\circ$), -0.04 kcal/mol (~ 7.5 Å, $\sim 25^\circ$) far lower than the optimized ground state at 0K. This could explain why *p*TPA-TRZ molecules have a wider distribution than TPA-TRZ. As in the earlier discussion, we suggested that the interaction between *p*TPA-TRZ is mainly van der Waals in origin. The contribution of van der Waals forces can be modelled using Buckingham potential or Lennard-Jones potential [30] and these potentials have an r^{-6} dependent. Van der Waals force of attraction becomes far weaker when intermolecular distance increases but becomes stronger when the area of interaction is large. However, coulombic interaction has a potential of r^{-1} dependent and hence, the partial localization of $2p_z$ electrons $-\pi$ deficient interaction remains intact. In photoexcitation in toluene, a wider range of conformational configurations of *p*TPA-TRZ are excited by the photons compared with TPA-TRZ.

The next question is what happen to the molecular conformation in excited states in the solvent? In order to answer this question, we proceed to carry out excited state QMD. In order to do that, we

sampled preferential molecular configurations performed in ground state QMD earlier and subjected the molecules to first excited state QMD. Figure 6(c) and Figure 6(d) show the excited state TPA-TRZ and *p*TPA-TRZ probability density distribution versus radial angle respectively for molecular initial configurations of (7 Å, 55°) for TPA-TRZ and (5.5 Å, 15°) for *p*TPA-TRZ. Firstly, we noticed that the intermolecular distance is reduced in both TPA-TRZ and *p*TPA-TRZ. Furthermore, the excited complex adopted more confined molecular configurations. TPA-TRZ exhibits two preferential orientations. Closer examination of the dynamics revealed that TRZ can rotate around its axis (see electronic media *ptpa-trz.mpeg*). In excited state, the electron is located at TRZ and hole is located in TPA/*p*TPA. The coulombic interaction between hole and electron enhances the confinement of the dimers resulting a shorter intermolecular distance. Due to stronger coulombic interaction which act as a restoring force, any external jostling such as collisions from solvent molecules, will eventually bring the dimers in equilibrium positions. Excited state QMDs are also carried out with other less dominant ground state molecular configurations. We found out that excited state *p*TPA-TRZ can exhibit a wide range of intermolecular distance from 3.8 Å to 5.3 Å (see supplementary information Figure S5 and S6) Since, the energy of the lowest charge transfer excited state is a function of intermolecular distance [31], in *p*TPA-TRZ, the emission is broadened modulated with peaks corresponding to dominant conformational distribution.

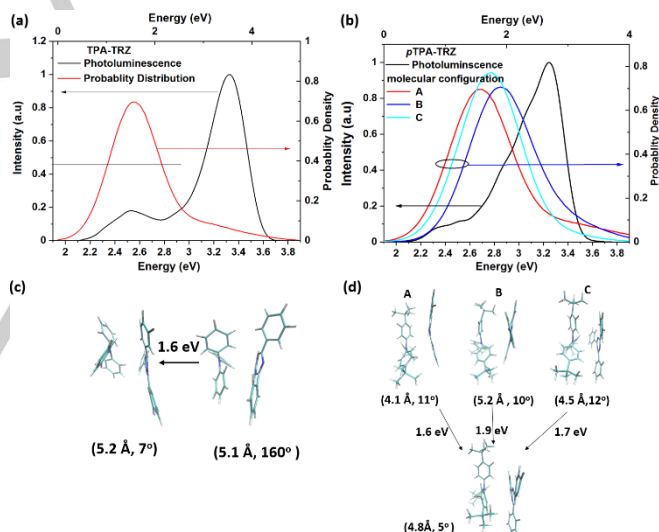


Figure 7. The photoluminescence spectra and the 0-0 transition energies probability distributions for (a) TPA-TRZ (b) *p*TPA-TRZ. The molecular structures of 0-0 transition at the peak of the distributions for (c) TPA-TRZ (d) *p*TPA-TRZ along with their intermolecular distances and angles

The 0-0 transition energy can be calculated by subtracting the excited state energy of the molecule with the ground state of that molecule. Each energy obtained from the excited state of TPA-TRZ in QMD in Figure 6(c) are subtracted by list of energies obtained from the ground state in Figure 6(a). From this, we generated 10 million possible 0-0 transition energies and a probability density can be plotted. The structures that contribute to the peak of distribution can be extracted out. The same method can be repeated for *p*TPA-TRZ. Figure 7(a) and (b) shows the photoluminescence spectra and the distributions of 0-0 transition energies for TPA-TRZ and *p*TPA-TRZ. Note that current DFT theory tends to underestimate the transition energies [32] and

ARTICLE

hence, the upper y-axes in Figure 7(a) and 7(b) are referred to the energy obtained from the simulations while the bottom y-axes are the experimental values. The full width half maximum (FWHM) for the simulated curve for Figure 7(a) is ~ 0.8 eV while for Figure 7(b) the FWHM is ~ 1.1 eV. Such broadening is related to the disorder in the molecular conformations [33]. The molecular conformations that are responsible for the 0-0 transitions are given in Figure 7(c) and Figure 7(d) for TPA-TRZ and *p*TPA-TRZ respectively. As we can see, because of the weaker interaction for *p*TPA-TRZ at 300K, molecules can adopt different preferential orientations at the ground state. A, B and C are obtained from subtracting excited energies from Figure S5(c), Figure 6(d) and Figure S5(d) respectively with the ground state energies in Figure 6(b). This is selected to illustrate that different conformations of molecular complexes can result in different emission wavelengths. The peaks of 0-0 transitions depend on the excited geometry as shown in Figure 7(d). The 0-0 transition energies decrease with decreasing excited state intermolecular distance as shown in Figure 7(d).

Another question is, as revealed in QMD in the TPA-TRZ dimer, why the radial angle between TPA and TRZ is not near zero in contrast to ground state optimized DFT calculations? It is also important to note that in the mixture of TPA and TRZ with equal molar ratio, we expect not all TPA will be dimerized with TRZ. Most likely, only a small fraction of them will. We carried out classical molecular dynamics (MD) by explicitly including the solvent molecules which cannot be done using QMD due to very high computational cost. Starting with the initial conditions which are well-dispersed, the final optimized MD structures for TPA (cyan)-TRZ (orange) and TPA(cyan)-*p*TRZ(orange) are shown in Figure 8(a) and Figure 8(b) respectively with the embedded toluene (yellow) molecules. It appeared that it has aggregated with size between 30 Å - 60 Å but the solvent molecules are also appeared inside the aggregate. Toluene plays an important role by affecting the intermolecular orientation of supramolecules TPA-TRZ and *p*TPA-TRZ through a solvation process between toluene and compound, which may reflect and induce specific interactions involved [34]. As for toluene naturally is a nonpolar/apolar organic solvent, it does affect the morphology of compounds TPA-TRZ and *p*TPA-TRZ through co-assembly happened to form an aggregate as shown in Figure 8(a) and 8(b). Figure 8(c) and Figure 8(d) are the conformers in stick model from MDs with solvent molecules removed with the color scheme corresponding to the nearest pair of interactions. For clarity, the interaction pairs are given in Figure 8(e) and Figure 8(f). Figure 8(e) shows a ring staggered (yellow bar in Figure 8(e)), T-shaped (blue bar), end-to-end for donor and acceptor pair (purple bar) and off aligned face to face (green bar) for TPA-TRZ. None has near zero radial angle. As previously shown in Figure 4(a), π - π interactions can be seen in the three phenyl rings of TPA with TRZ. However, in MD, we can see that only one of the phenyl rings from TPA is involved in π - π interactions. This is also similar with QMD where the center of triazine ring doesn't stack on top of the nitrogen atom of TPA, similar to the explicit solvent in MD, we observed more pi-pi interaction of phenyl group in TPA and TRZ. With combination of attractive force from the partial localization of $2p_z$ electrons - π deficient interaction and π - π interactions, the dimer is unlikely to stack completely face to face with each other when there is a greater freedom of motion. The formation of excited charge transfer state depends on the mutual orientation and distance of the molecules [35]. For spatially separated excited

charge transfer states, the oscillatory strength depends on certain degree of electronic wavefunction overlap. Besides, the intermolecular distance plays an important role, the degree of face-to face overlapping is also important for excitation of spatially separated charge transfer states. Hence, the T-shaped and end-to-end for donor and acceptor pair are unlikely to participate in excited charge transfer states leaving with off-aligned TPA-TRZ with certain degree of π - π stacking interactions to be the main excited charge transfer state conformer. For *p*TPA-TRZ, the staggered conformation was not observed due to the methyl group in *p*TPA. We also observed that there are more toluene molecules acting as an inter-linkages or bridges involved in the interaction for TPA-TRZ than *p*TPA-TRZ system. We found no distinct conformer for *p*TPA-TRZ system. Since QMD treats the interactions intrinsically while MD uses parameterized force field, the two methods are unlikely to give identical results, however, both methods showed the lack of distinct conformers for *p*TPA-TRZ.

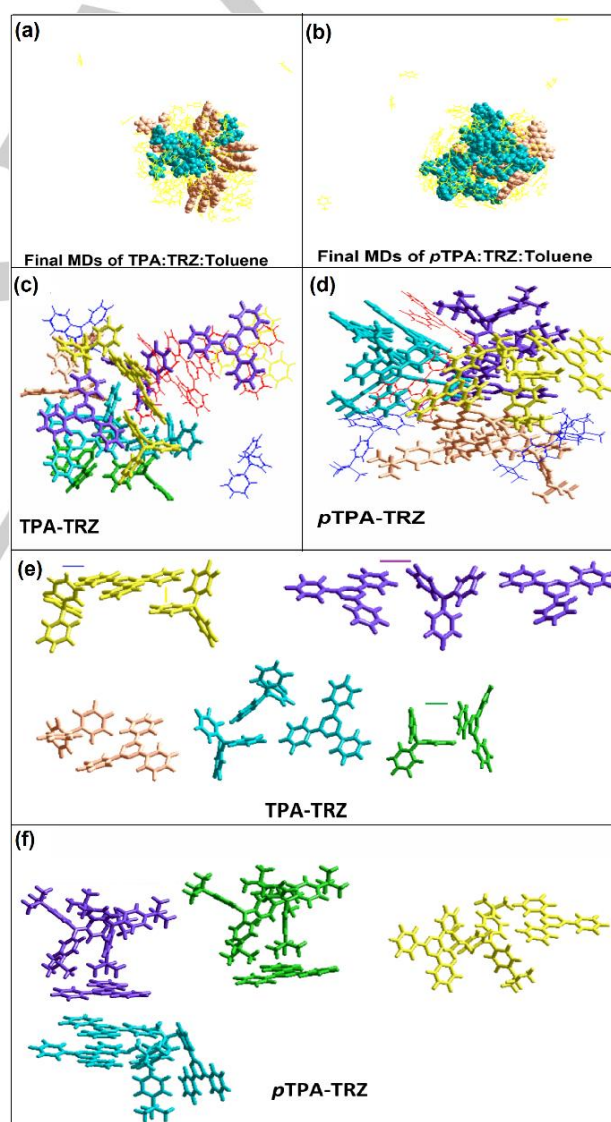


Figure 8. Final optimized MD structures in ball model TRZ (orange) and toluene (yellow) and (a) TPA, (b) *p*TPA (cyan), (c) conformers in stick model for (c) TPA-TRZ (d) *p*TPA-TRZ in toluene (not shown) (e) list of conformers with the nearest molecules with corresponding colors in (c) and (d) for (e) TPA-TRZ and (f) *p*TPA-TRZ

ARTICLE

Conclusion

The formation of heterodimer between TPA and TRZ is encouraged by the interaction between partial localization of $2p_z$ electrons in the nitrogen atom of TPA and π electron deficient in triazine and the π - π stacking interactions between phenyl groups. However, such interactions can be destroyed by introducing *tert*-butyl group as a bulky side groups at *para*- position in TPA. The weakly bounded heterodimers formed between *p*TPA and TRZ adopt numerous conformational configurations in solvent in contrast to TPA-TRZ, with only one dominant conformer is found in QMD. As a result, emission from *p*TPA-TRZ heterodimers consist of numerous superimposed Gaussian peaks. One of the important implications that we can infer from such system, because of strong coulombic interaction between hole and electron in donor-acceptor system in the excited state, intermolecular distance is expected to reduce when there is sufficient face to face stacking between donors and acceptors. This will be accompanied by geometry relaxation after de-excitation contributing the loss of energy via molecular reorganizations in particularly if flexible bonds are connected between them.

Experimental Section

Characterization and measurements. Materials were characterized by means of ^1H and ^{13}C NMR spectroscopy using BRUKER AVN III 400 MHz FT-NMR spectrometer using deuterated chloroform as the solvent and TMS as internal standard.

Material Synthesis. Tris-(4-*tert*-butylphenyl)amine was synthesized using Friedel-Crafts alkylation reaction according to literature procedure [36]. Trifluoroacetic acid can be used for activation of *tert*-butyl alcohol. A mixture of triphenylamine (0.5 g), 2-methylpropane-2-ol (2 mL), and trifluoroacetic acid (10 mL) was stirred and refluxed for 24h. Then, the mixture was poured in 20% NaOH solution and the aqueous layer was extracted with dichloromethane. The organic layer was dried, filtered and the solvent was removed under vacuum. The precipitated was subjected to column chromatography using 100% heptane. The resulting white solid collected has a mass of 0.5865g (69 % yield). ^1H NMR (400 MHz, CDCl_3): δ 1.31 (s, 27H; C-(CH₃)₃), 7.01 (d, $J = 8.8$ Hz, 6H; Ar-H), 7.24 (d, $J = 8.8$ Hz, 6H; Ar-H), ^{13}C NMR (100 MHz, CDCl_3): $\delta = 31.7$ [(C-(CH₃)₃), 34.4 (C), 123.6 (Ar-CH), 126.1 (Ar-CH), 145.2 (Ar-C), 145.5 (Ar-C).

Photophysical properties. The UV-visible absorption spectra of the compounds in solutions of toluene at a concentration of 100 μM was observed using a Shimadzu UV-Vis spectrophotometer (UV-2600). The photoluminescence emission spectra of the compounds in solutions of cyclohexane and toluene at room temperature were characterized using a Perkin Elmer luminescence spectrophotometer with 325nm excitation wavelength.

Computational calculations. All molecular geometries are optimized using density functional calculations performed in Terachem 1.9 [37] using the optimally tuned range-separated [38] LC- ω PBE functional at cc-pVDZ basis level under polarizable continuum model (PCM) with toluene as a solvent [39]. The calculations were performed using a GPU server that had 64 GB RAM installed to support eight Tesla K10 graphic cards. The optimized geometries are then subjected to quantum molecular dynamics (QMD) simulations using the same functional theory except at 6-31g basis set. The initial temperature is set at 550K with equilibrium temperature of 300K using Langevin as a thermostat. Langevin is chosen to simulate the effect of jostling of solvents. The QMDs are carried out with 1 femtosecond (fs) time step with 100000 steps. The solvent radius is set to be 3.48 Å and

dielectric constant of 2.38, typical values for a toluene. Suitable molecules from ground state QMD are sampled to perform first excited state QMD using time dependent LC- ω PBE at same basis level. In order to establish the relevance to the experimental observations, the vertical absorption oscillatory strengths along with the probability densities of that particular orientations needed to be taken account. Hence, the mapping of Figure 6(a) is reduced from 50 x 50 matrix to 10 x 10 matrix and the products of vertical absorption oscillatory strengths and the probability densities, p , were calculated (see Table S2-S5 in supplementary information). The molecules with the highest product, p_{max} and up to $0.1p_{\text{max}}$ were selected for excited state QMD. Time-reversible integrator with dissipation is also implemented. The relevant data points are then extracted from the output files so that intermolecular distance and the angle formed by the two normal vectors defined in the manuscript can be calculated using Python 3.5 with the help of numpy and sympy modules. For initial configuration for molecular dynamics simulations of 10:10:60 molecules of TPA:TRZ:toluene and *p*TPA:TRZ:toluene were randomly distributed in the simulation box of 80.6 x 84.9 x 77.3 Å³ using a Packmol Program [40]. CHARMM force field and conjugate gradient algorithm were applied to optimize the energy until the convergence of 0.01 kcal/(Å mol) was obtained using HyperChem software. Series of molecular dynamics simulations were done using NVT ensemble. In the heating phase of 200 ps with 1 fs time step, the temperature of the system is increased from an initial value of 0 K to a final value of 300 K with temperature step of 10 K. Then, each system was kept at 300 K for another 400 ps using time step of 2 fs and the final complex structure was obtained for interaction analysis.

Conflicts of interest

There are no conflicts to declare

Acknowledgements

The authors gratefully acknowledge the funding by the University Malaya Research University Grant-Faculty Program (GPF046B-2018) and Dr. Hadieh Monajemi and Kheng Ghee Ng from Data Intensive Computing Centre of University Malaya for rentlessly maintaining the GPU servers. Also, the authors would like to thank Dr. Muhammad Faisal Bin Khyasudeen for the technical discussion.

Keywords: dimer • donor • acceptor • TADF • conformer

References

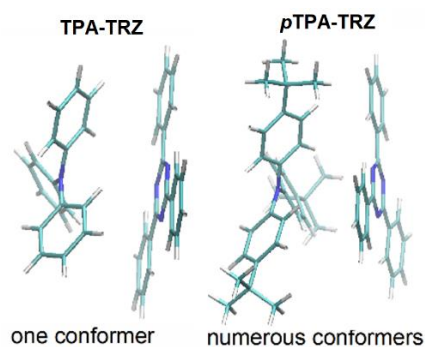
- [1] N. Hayashi, A. Kanda, H. Higuchi, K. Ninomiya in *Topics in Heterocyclic Chemistry, Vol. 18* (Eds.: K. Matsumoto, N. Hayashi), Springer, **2009**, pp. 1-35.
- [2] Y. S. Wang, J. Yang, Y. Tian, M. M. Fang, Q. Y. Liao, L. W. Wang, W. P. Hu, B. Tang, Z. Li, *Chem Sci* **2020**, *11*, 833-838.
- [3] M. K. Etherington, N. A. Kukhta, H. F. Higginbotham, A. Danos, A. N. Bismillah, D. R. Graves, P. R. McGonigal, N. Haase, A. Morherr, A. Batsanov, C. Pflumm, V. Bhalla, M. R. Bryce, A. P. Monkman, *J Phys Chem C* **2019**, *123*, 11109-11117.
- [4] K. L. Woon, Z. A. Hasan, B. K. Ong, A. Ariffin, R. Griniene, S. Grigalevicius, S. A. Chen, *Rsc Adv* **2015**, *5*, 59960-59969.
- [5] V. Jankus, A. P. Monkman, *Adv Funct Mater* **2011**, *21*, 3350-3356.
- [6] B. Feringan, P. Romero, J. L. Serrano, C. L. Folcia, J. Etxebarria, J. Ortega, R. Termine, A. Golemme, R. Gimenez, T. Sierra, *J Am Chem Soc* **2016**, *138*, 12511-12518.
- [7] M. Carini, M. Marongiu, K. Strutynski, A. Saeki, M. Melle-Franco, A. Mateo-Alonso, *Angew Chem Int Edit* **2019**, *58*, 15788-15792.
- [8] Z. H. Zong, P. Z. Li, A. Y. Hao, P. Y. Xing, *J Phys Chem Lett* **2020**, *11*, 4147-4155.

ARTICLE

- [9] C. Tschierske, *Angew Chem Int Edit* **2013**, *52*, 8828-8878.
- [10] C. D. Jia, H. H. Miao, B. P. Hay, *Cryst Growth Des* **2019**, *19*, 6806-6821.
- [11] J. Novotny, S. Bazzi, R. Marek, J. Kozelka, *Phys Chem Chem Phys* **2016**, *18*, 19472-19481.
- [12] A. Reyes, L. Fomina, L. Rumsh, S. Fomine, *Int J Quantum Chem* **2005**, *104*, 335-341.
- [13] T. J. Mooibroek, P. Gamez, *Inorg Chim Acta* **2007**, *360*, 381-404.
- [14] J. S. Costa, A. G. Castro, R. Pievo, O. Roubeau, B. Modéc, B. Kozlevcar, S. J. Teat, P. Gamez, J. Reedijk, *Crystengcomm* **2010**, *12*, 3057-3064.
- [15] X. J. Wan, C. X. Li, M. T. Zhang, Y. S. Chen, *Chem Soc Rev* **2020**, *49*, 2828-2842.
- [16] A. Wadsworth, M. Moser, A. Marks, M. S. Little, N. Gasparini, C. J. Brabec, D. Baran, I. McCulloch, *Chem Soc Rev* **2019**, *48*, 1596-1625.
- [17] N. Bunzmann, S. Weissenseel, L. Kudriashova, J. Gruene, B. Krugmann, J. V. Grazulevicius, A. Sperlich, V. Dyakonov, *Mater. Horiz.*, **2020**, *7*, 1126-1137
- [18] Y. C. Liu, C. S. Li, Z. J. Ren, S. K. Yan, M. R. Bryce, *Nat Rev Mater* **2018**, *3*.
- [19] J. J. Liu, D. Z. Lu, Y. F. Chen, Y. T. Dong, Z. Yang, *Dalton Trans.*, **2015**, *13*, 5957-5960.
- [20] Y. K. Wang, C. C. Huang, H. Ye, C. Zhong, A. Khan, S. Y. Yang, M. K. Fung, Z. Q. Jiang, C. Adachi, L. S. Liao, *Adv Opt Mater* **2020**, *8*, 1901150.
- [21] E. Spuling, N. Sharma, I. D. W. Samuel, E. Zysman-Colman, S. Brase, *Chem Commun* **2018**, *54*, 9278-9281.
- [22] M. Auffray, D. H. Kim, J. U. Kim, F. Bencheikh, D. Kreher, Q. S. Zhang, A. D'Aleo, J. C. Ribierre, F. Mathevet, C. Adachi, *Chem-Asian J* **2019**, *14*, 1921-1925.
- [23] T. Lu, F. W. Chen, *J Comput Chem* **2012**, *33*, 580-592.
- [24] T. Lu, F. W. Chen, *J Mol Graph Model* **2012**, *38*, 314-323.
- [25] T. Lu, F. W. Chen, *J. Theor. Comput Chem*, **2012**, *11*, 163-183
- [26] H. Méndez, G. Heimel, S. Winkler, J. Frisch, A. Opitz, K. Sauer, B. Wegner, M. Oehzelt, C. Röthel, S. Duhm, D. Többens, N. Koch, *Nat. Commun.*, **2015**, *6*, 8560
- [27] E. R. Johnson, S. Keinan, P. Mori-Sánchez, J. Contreras-García, A. J. Cohen, W. Yang, *J. Am. Chem. Soc.* **2010**, *132*, 6498-6506
- [28] K. L. Woon, C. L. Yi, K. C. Pan, M. K. Etherington, C. C. Wu, K. T. Wong, A. P. Monkman, *J Phys Chem C* **2019**, *123*, 12400-12410.
- [29] N. Berger, L. J. B. Wollny, P. Sokkar, S. Mittal, J. Mieres-Perez, R. Stoll, W. Sander, E. Sanchez-Garcia, *Chemphyschem*, **2019**, *20*, 1664-1670
- [30] T. C. Lim, *Z Naturforsch A* **2009**, *64*, 200-204.
- [31] Y. Fang, S. L. Gao, X. Yang, Z. Shuai, D. Beljonne, J. L. Bredas, *Synthetic Met* **2004**, *141*, 43-49
- [32] T. J. Penfold, Dias F. B., A. P. Monkman, *Chem Commun* **2018**, 3926-3935
- [33] Serevicius T, Skaisgiris R, Dodonova J, Kazlauskas K, Jursenas S, Tumkevicius S *Phys. Chem. Chem. Phys.*, **2020**, *22*, 265-272
- [34] S. Xue, P. Xing, J. Zhang, Y. Zeng, Y. Zhao, *Chemistry—A European Journal* **2019**, *25*, 31, 7426-7437
- [35] A. Aster, G. Licari, F. Zinna, E. Brun, T. Kumpulainen, E. Tajkhorshid, J. Lacour, E. Vauthey, *Chem. Sci.* **2019**, *10*, 10629-10639
- [36] D. Vak, J. Jo, J. Ghim, C. Chun, B. Lim, A. J. Heeger and D.-Y. Kim, *Macromolecules*, **2006**, *39*, 6433-6439.
- [37] I. S. Ufimtsev, T. J. Martínez, *J. Chem. Theo. Comp.*, **2009**, *5*, 2619
- [38] H. T. Sun, C. Zhong, J. L. Bredas, *J Chem Theory Comput* **2015**, *11*, 3851-3858.
- [39] F. Liu, N. Luehr, H. J. Kulik, T. J. Martinez, *J. Chem. Theory Comput.* **2015**, *11*, 7, 3131-3144
- [40] L. Martínez, R. Andrade, E. G. Birgin, J. M. Martínez, *J Comput Chem.* **2009**, 2157-2164

ARTICLE

Entry for the Table of Contents



one conformer

numerous conformers

Functionalizing TPA with tris-(4-(tert-butyl) as tris(4-(tert-butyl)phenyl)amine (pTPA) decreases the strength of attractive interactions in toluene. The weakly bounded pTPA and TRZ adopt numerous conformations resulting in emissions from different excited charge-transfer conformers.